Journal of Japan Association for Earthquake Engineering, Vol.15, No.3, 2015

MODAL IDENTIFICATION OF A HEAVILY DAMAGED NINE-STORY STEEL-REINFORCED CONCRETE BUILDING BY AMBIENT VIBRATION MEASUREMENTS

Kahori IIYAMA[1], Satoshi KURITA[2], Masato MOTOSAKA[3], Kazuki CHIBA[4], Hiroki HIRAMATSU[5] and Kazuya MITSUJI[6]

[1] Member of JAEE, Researcher, Information Science and Engineering, Tokyo Institute of Technology, Tokyo, Japan, iiyama.k.aa@m.titech.ac.jp
[2] Member of JAEE, Professor, Department of Architecture, Tokyo University of Science, Tokyo, Japan, kurita@rs.kagu.tus.ac.jp
[3] Member of JAEE, Professor, International Research Institute of Disaster Science, Tohoku University, Miyagi, Japan, motosaka@irides.tohoku.ac.jp
[4] Member of JAEE, Researcher, Tokyu Construction Co., Ltd., Institute of Technology, Kanagawa, Japan, chiba.kazuki@tokyu-cnst.co.jp
[5] Tokyo Soil Research Co., Ltd., Tokyo, Japan, hiramatsu@tokyosoil.co.jp
[6] Member of JAEE, Associate Professor, Department of Education, Art and Science, Yamagata University, Miyagi, Japan, mitu@e.yamagata-u.ac.jp

ABSTRACT: Modal parameters of a nine-story steel-reinforced concrete building damaged heavily by the 2011 off the Pacific coast of Tohoku Earthquake were identified from ambient vibration data using frequency domain decomposition (FDD). The characteristics of the identified three-dimensional mode shapes, torsional component of the mode and deformation ratio of the mode were discussed with respect to the seismic damages. In addition, we identified the mode shapes by two kinds of FDD: one for a general viscous damping system, and the other for a proportional damping system. The influence of a viscous damping condition on the identified mode shapes was discussed.

Key Words: Microtremor measurement, Damage estimation, System identification, Frequency domain decomposition

1. INTRODUCTION

In structural health monitoring, many methods are available for detecting damage using ambient vibration records measured before and after earthquakes. Ambient vibration-based methods are preferable to earthquake record–based methods in that ambient vibration can be measured any day. In addition, many locations in a building or structure can be examined by a movement measurement[1)] using a limited number of instruments. Thus, the effectiveness of ambient vibration–based methods in examining damage to buildings has gained increasing attention.

Some methods for detecting and locating damage are based on vibrational theory and use changes

in modal properties before and after damage, but the theoretical assumptions on which the vibration systems used in these methods differ depending on the method. One of the differences is the assumption regarding the input source of ambient vibration. Vibrational theory can be categorized into two cases depending on the input source: one assumes that the vibration source is only ground excitation[2)-3)], and the other assumes that there are other sources in addition to ground excitation, e.g., wind-force[4)-11)]. The latter case regards the inputs as unknown and identifies modal parameters using only outputs (measurement records). In ambient vibration measurements, the influence of fluctuating wind pressure cannot be ignored sometimes[12)-15)], especially for high-rise structures. However, so far, the decomposition of the vibration record into waves caused by ground motion and those caused by fluctuating wind pressure has proved difficult. Therefore, it is better to employ methods that use only outputs if several kinds of input sources seem to exist.

Another difference is the assumption of the structural damping model. Ambient vibration based methods can be categorized into two types depending on the damping system used: one assumes a non-proportional damping system and identifies complex modes[4)-10)], and the other assumes a proportional damping system and identifies the real number of modes[3), 11)]. However, the influence of the difference in the employed damping system on identification results has not been investigated. The examination of this influence is necessary to increase the reliance of damage detection.

Damaged parts are detected based on damage indices calculated from identified modal properties. The inter-story stiffness of a one-dimensional shear model has been heavily used as a damage index because it is easy to use. However, a one-dimensional shear model cannot necessarily be applied to all types of buildings. For example, for a high-rise or an irregularly shaped building, the natural frequencies of high-order modes calculated by using one-dimensional models are clearly different from those calculated by using three-dimensional models. In addition, identification errors were observed in a study examining changes in the inter-story stiffness of an actually damaged building before and after retrofitting[16)] because the vibrational properties in the three-dimensional mode were ignored. On the other hand, Hamamoto et al.[5)] proposed a damage detection method using the torsional mode and demonstrated the effectiveness of the proposed method by a model experiment. Thus, utilizing three-dimensional vibration characteristics can possibly improve the accuracy of building damage detection. However, the three-dimensional vibration characteristics of damaged buildings have not been determined because there are few studies based on existing damaged buildings.

In this study, the ambient vibrations of a nine-story steel-reinforced concrete (SRC) building that was heavily damaged by the 2011 Tohoku earthquake were measured by using a high-density array. The building's modal properties were identified by frequency domain decomposition (FDD), which is an output-only technique. Based on the identified modal parameters, the three-dimensional mode shapes, torsional deformation, distribution patterns of the slope of the mode shape, and the changes in the natural frequency of the first-order modes over time were evaluated. The relationship between these characteristics and the damage level was discussed. In addition, the properties of complex eigenmodes identified from ambient vibration records are examined.

2. BUILDING SELECTED FOR STUDY

The building selected for the study was a nine-story SRC building belonging to Tohoku University in

Photo.2.1 Building selected for study

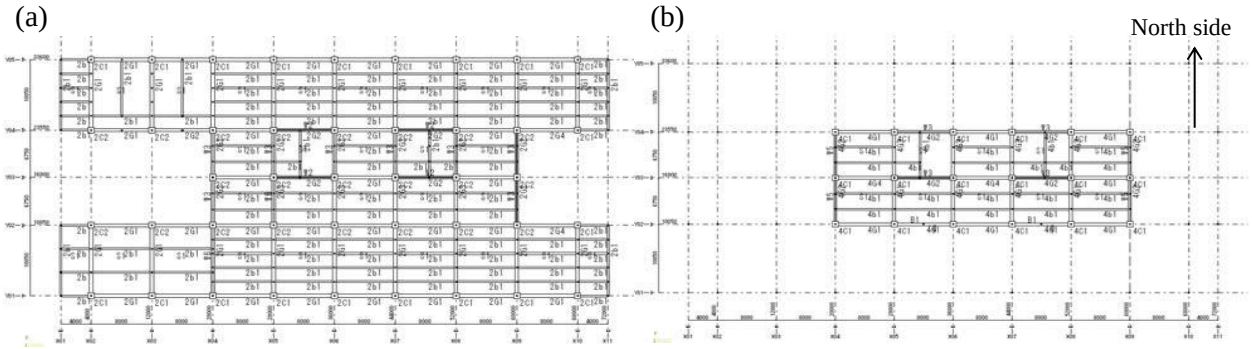

Figure 2.1 Floor plan: (a) lower floors (first and second floors) and (b) upper floors

Table 2.1 Summary of building damages after completion and reinforcement works

Mongh and Year	Event	building damages and reinforcement works
March, 1969	Completion of construction	
June, 1978	Miyagiken-oki earthquake	The maximum acceleration (1040 cm/s^2) was observed on the ninth floor. The maximum width of bending and shear cracks [17] was approximately 1 mm at the side wall on the third and fourth floors, and approximately 1.5 mm at the beams.
July, 2000	Beginning of seismic retrofit	Replacement of concrete side walls, reinforcement of floor slabs, reinforcement of beams by steel plate wraps, and installation of steel braces
March, 2001	End of seismic retrofit	
March, 2011	Tohoku earthquake	The four corner columns on the third floor were heavily crushed. The maximum acceleration of 903 cm/s^2 was observed on the ninth floor.
May, 2011	Emergency rehabilitation	Reinforcement of the four columns Installation of earthquake-resistant shear walls in the corner of the third floor in the longitudinal direction

Sendai, Japan (Photo 2.1). It was constructed in 1969 on a pile foundation with moment-resistant frames and shear walls. The structure consisted of a 32.9-m-tall nine-story building and two-story pilotis along both sides of the building. The building often experienced major earthquakes and was once retrofitted from July 2000 over six months. The 2011 Tohoku earthquake heavily damaged the building, and emergency rehabilitation was carried out two months later. A summary of the building damages after completion of construction and reinforcement works is shown in Table 2.1. Fig. 2.1 shows the plan of the lower and upper floors. The span for the longitudinal (*LG*) direction is 8.0 m for both the lower and upper floors, and that in the transversal (*TR*) direction is 10.05 m and 6.75 m for the lower and upper floors, respectively.

2.1 Details of structure at completion and damage caused by 1978 Miyagiken-oki Earthquake

At the completion of construction, the building structure had ramen frames in which earthquake-resistant shear walls were installed in both the *TR* and *LG* directions. The details of the member sections and layout are available in a previous paper[17]. The main elements installed on the upper floors could resist strong earthquakes (Fig. 2.1(b)): the multi-story and multi-span shear walls on both the gable sides and the multi-story shear walls around the stair halls on the north side. The elements were balanced in the *TR* direction, but unbalanced in the *LG* direction because the earthquake-resistant walls were weighted toward the north side of the building.

When the building experienced the Miyagiken-oki earthquake in June 1978, the maximum acceleration (1040 cm/s^2) was observed on the ninth floor. According to a report by Shiga et al.[17], many cracks were found at the shear walls (shear cracks) and the corner columns (bending cracks) between the third and fourth floors; the maximum width of these cracks was 1 mm. In addition, shear cracks were found on the beams at the top and bottom of the earthquake-resistant walls, the maximum width of these cracks was around 1.5 mm.

2.2 Seismic retrofitting

Seismic retrofitting was carried out from July 2000 to March 2001. A schematic of the retrofitting is shown in Fig. 2.2. The east and west side walls on the third and higher floors were replaced by new concrete walls. The thickness of the walls on the sixth and higher floors was increased by 30 cm. The strength of concrete was 27 N/mm^2, which is 6 N/mm^2 greater than that before the retrofitting. Floor slabs adjoining the side wall were reinforced and became thicker. The beams adjoining the stair halls were wrapped using steel sheets. To decrease the stiffness eccentricity in the *LG* direction, the structural frames on the south side were strengthened by installing steel braces from the third to the eighth floor. The details of the seismic performance after the retrofitting are presented in Table 2.2. The index "Is" in the table is the value assessed by the third diagnostic procedure in accordance with the seismic diagnosis standard provided by the Japan Building Disaster Prevention Association.

Table 2.2 Seismic performance after retrofitting[18)]

	Is (structural seismic diagnosis index)								
	1FL	2FL	3FL	4FL	5FL	6FL	7FL	8FL	9FL
Transversal (*TR*)	0.75	0.88	0.84	1.01	1.02	1.05	1.13	1.33	1.32
Longitudinal (*LG*)	0.63	1.12	1.45	0.88	0.84	0.93	1.02	1.20	1.07

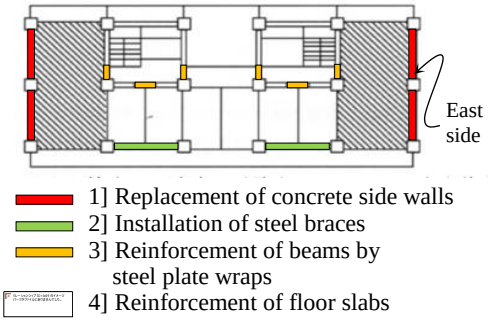

Figure 2.2 Seismic retrofitting from July 2000 over six months (Motosaka et al., 2002)

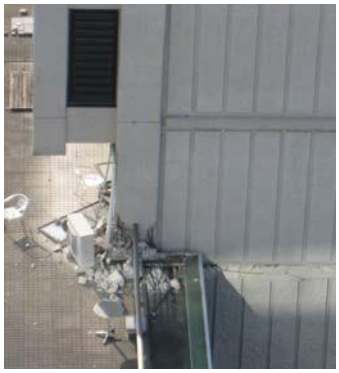

Photo 2.2 Damage to columns (on third floor)

Photo 2.3 Emergency rehabilitation (on third floor)

2.3 Damage caused by 2011 Tohoku earthquake and emergency rehabilitation

During the 2011 Tohoku Earthquake, the maximum acceleration (903 cm/s^2) was observed on the ninth floor. The main shock caused all the corner columns on the third floor to crash with rocking vibration (Photo 2.2). According to the post-earthquake damage evaluation reported by Sakota et al[19)], the damage on the third floor in the *TR* direction was the most severe. The aseismatic residual ratio R was 23%, and the damage level was categorized as "seriously damaged." Emergency rehabilitation was carried out in May 2011. The four crashed corner columns were reinforced, and shear walls were additionally installed along the longitudinal side, adjacent to each corner column (Photo 2.3).

3. METHOD FOR MODAL IDENTIFICATION

FDD was applied to identify the modal property of the building. To examine the damping property of the building, two kinds of FDD were employed: one proposed by Brincker et al.[9),10)], which is based on the theory of a non-proportional damping system and the other proposed by Iiyama and Kurita[11)], which is based on the theory of a proportional damping system. Both techniques use the power spectral density (PSD) matrix [*G*] calculated from ambient vibration records.

Let $y_i(t)$ be the time series measured at point i and $Y_i(j\omega)$ be the Fourier transforms of $y_i(t)$; then the PSD matrix [*G*] can be given by

$$[G(j\omega)] = E[\{\bar{Y}(j\omega)\}\{Y(j\omega)\}^T] \tag{3.1}$$

where ω is the circular frequency, j denotes an imaginary unit, $E[\ ]$ denotes the ensemble average, index $^-$ denotes a complex conjugate, and superscript T denotes transposition. Let N be the total number of measurement points; then, column vector $\{Y(j\omega)\}$ can be represented by

$$\{Y(j\omega)\} = \{Y_1(j\omega), ..., Y_N(j\omega)\}^T \tag{3.2}$$

Brincker et al. decomposed the complex conjugate of $[G]$ with respect to each frequency by singular value decomposition.

$$[\bar{G}(j\omega)] = [U(j\omega)][S(j\omega)][U(j\omega)]^H = \sum_{i=1}^{N} s_i(j\omega)\{U_i(j\omega)\}\{U_i(j\omega)\}^H \tag{3.3}$$

where superscript H denotes a complex conjugate and transpose, and $s_i(j\omega)$ and $\{U_i(j\omega)\}$ represent singular values and singular vectors, respectively. Let the maximum singular value be the first singular value $s_1(j\omega)$, and the corresponding singular vector be the first singular vector $\{U_1(j\omega)\}$.

Brincker et al.[9] introduced the following approximation of $[G]$ around $\omega = \omega_r$ under a non-proportional damping system subjected to white noise excitation:

$$[\bar{G}(j\omega)] \approx a_r(j\omega)\{\phi_r\}\{\phi_r\}^H \ , \ \ a_r(j\omega) = \mathrm{Re}\left(\frac{2d_r}{j\omega - \lambda_r}\right) \tag{3.4}$$

where d_r is a constant value relevant to white noise excitations and $\{\phi_r\}$ is the rth complex mode shape vector of the system. λ_r is the pole represented by the sum of the rth modal damping ratio σ_r and rth damping circular frequency ω_{dr}:

$$\lambda_r = -\sigma_r + j\omega_{dr} \tag{3.5}$$

A comparison of Eq. (3.3) and Eq. (3.4) shows that $s_1(j\omega)$ and $\{U_1(j\omega)\}$ are equivalent to a_r and $\{\phi_r\}$, respectively. Considering these equivalencies, the eigenfrequency is identified as ω_r, which shows one of the peaks for $s_1(j\omega)$; the rth eigenmode is identified as $U_1(j\omega_r)$. In addition, the modal damping factor h_r is simply estimated from the single-degree-of-freedom autocorrelation function obtained by performing an inverse Fourier transform on $s_1(j\omega)$ around $\omega = \omega_r$.

Iiyama and Kurita[11] reconstructed the technical background of FDD and approximated $[G]$ to evaluate the influence of existing sth modes ($s \neq r$) on the identification accuracy of rth modal parameters. Based on the background, they proposed to use the real part of $[G]$ to identify the modal parameters for a proportional damping system. Similar to Eq. (3.3), the real part of $[G]$ can be decomposed by spectral decomposition.

$$[G^R(j\omega)] = [P(j\omega)][Q(j\omega)][P(j\omega)]^T = \sum_{i=1}^{N} q_i(j\omega)\{p_i(j\omega)\}\{p_i(j\omega)\}^T \tag{3.6}$$

where superscript R represents the real part of a complex matrix and $q_i(j\omega)$ and $\{p_i(j\omega)\}$ are the ith eigenvalue and the corresponding eigenvector, respectively. Spectral decomposition decomposes Hermitian matrices into eigenvectors and can also be applied to a real and symmetrical matrix. Let the maximum eigenvalue be the first eigenvalue $q_1(j\omega)$, and the corresponding eigenvector be the first eigenvector $\{p_1(j\omega)\}$.

For the proportional damping system subjected to white noise excitation, the approximation of $[G^R]$ around the rth circular frequency ω_r is given by

$$[G^R(j\omega)] \approx 2a_{rr}^p(j\omega)\left(\{\phi_r\} + \{\Delta_r^p(j\omega)\}\right)\left(\{\phi_r\} + \{\Delta_r^p(j\omega)\}\right)^T \tag{3.7}$$

$$2a_{rr}^p(j\omega) = \frac{c_{rr}}{\sigma_r^2 + (\omega - \omega_{dr})^2} = a_r(j\omega) \tag{3.8}$$

where c_{rr} is a constant relevant to white noise excitation, $\{\phi_r\}$ is the rth real eigenmode of the system, and $\{\Delta_r^p(j\omega)\}$ is an error vector relevant to the existing close modes[11]. Iiyama and Kurita demonstrated that $\{\Delta_r^p(j\omega)\}$ takes the smallest value at $\omega = \omega_{dr}$ and decreases when the difference

between ω_r and ω_s ($s \neq r$) increases. The procedures to identify the eigenfrequency, eigenmode, and modal damping are almost the same as those used by Brincker et al.

4. IDENTIFICATION OF MODAL PROPERTY FOR AMBIENT VIBRATION

4.1 Measurement

To examine the three-dimensional vibrational mode and locate the damaged parts, simultaneous high-density array measurements of ambient vibrations were performed in September 2011, October 2011 and January 2012. This study used only the third measurement records. The location of accelerometers is shown in Fig.4.1. The accelerometers were set at three locations (NW, SW, and NE) on each floor. Thirty portable accelerometers were used: 23 GPL-6A3P sensors from Mitutoyo Co. and seven JU210 sensors from Hakusan Co.. The ambient vibrations were recorded continuously for 60 min, at a sampling frequency of 200 Hz.

PSD and cross spectrum density (CSD) functions were calculated from ensemble average of 43 sample waves that were continuously cut from the records. The number of data points in a sample wave was 16384.

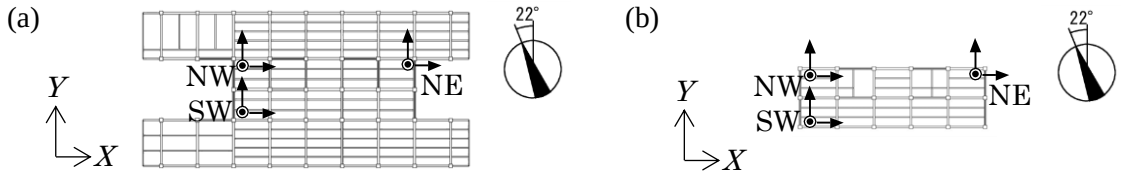

Figure 4.1 Location of accelerometers and indices: (a) first and second floors (lower floors), (b) floors above second floor (upper floors)

4.2 Time synchronization

Although the inner clocks of the accelerometers were synchronized using a GPS system just before being set up at each location, the time delays of the clocks gradually increased during the measurements. The relative time lags between the measurement records can be seen in the CSD function as the linear phase. Fig. 4.2(a) shows an example of the phase difference between the records on the roof and on the eighth floor at location NE in the *LG* and up-down (*UD*) directions. The relative time lags emerge as a straight line with a slope of $-2\pi\tau_0$ on the phase. In particular, the slope in the *UD* direction can be clearly seen for the frequency range of 2–10 Hz. If there is no relative time lag between two sensors ($\tau_0 = 0$), the phases are nearly equal to zero at low frequencies because floor slabs and columns may behave rigidly at frequencies lower than the first eigenfrequency. The optimal relative time lag τ_0 can be calculated by fitting the phases to $\theta(f) = 2\pi\tau_0 f$ by the least-squares method in the straight line frequency range. Fig. 4.2(b) shows the phases after the time correction. The phases were nearly equal to zero at low frequencies.

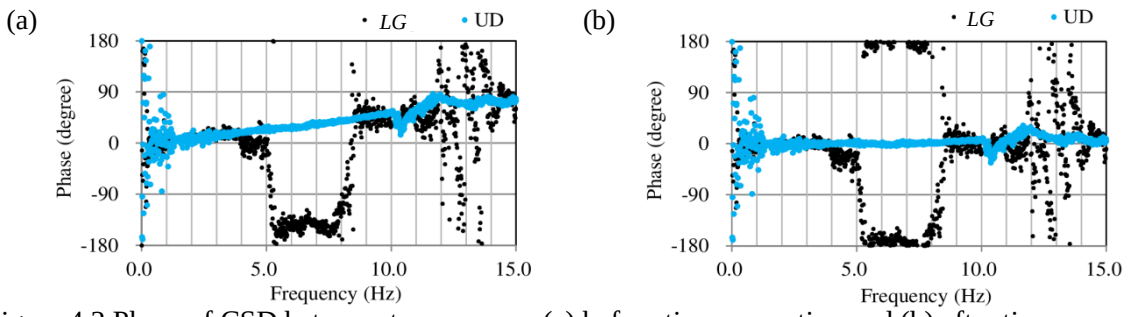

Figure 4.2 Phase of CSD between two sensors: (a) before time correction and (b) after time correction

4.3 Three-dimensional mode shape

If the in-plane rigidity of a floor slab is sufficiently high, it is possible to examine the transversal and torsional modes from the analysis model assuming one floor to be one mass point. Therefore, we calculated the three-dimensional modes of an in-line multi-degree-of-freedom (MDOF) model from the eigenmodes identified from FDD under the assumption that the floor slab is sufficiently rigid. Using both the eigenmodes identified through FDD and the three-dimensional modes, the properties of the eigenmodes of the damaged building are discussed. For the identification, the two horizontal acceleration records measured by 30 accelerometers (shown in Fig.4.1) were used.

4.3.1 Calculation method for three-dimensional mode

The methods used to calculate the three-dimensional modes of the in-line MDOF model are introduced by assuming each floor slab to be a rigid body. Hereafter in this paper, a floor is called as a *layer* and the floor of the first story is defined as the first layer. A section between the upper and lower layers is called as a *story*.

The representative point on a layer is denoted by the coordinate (x_c, y_c). The point is usually set to the center of gravity of the layer. The eigenmode at the representative point is represented by three components: the two translational components (u_x^C, u_y^C) and the rotational component u_T. It is supposed that there are N_m measurement points on the layer, and the eigenmode values are obtained at all the measurement points. The two translational components of the eigenmode on the measurement point j (x_j, y_j) is denoted as (u_x^j, u_y^j). The square error J of the difference between N_m identified modes and the calculated eigenmode at the representative points is obtained as

$$J(u_x^C, u_y^C, u_T) = \sum_{j=1}^{N_m} \left[\left\{ (u_x^C - (y_j - y_c)u_T) - u_x^j \right\}^2 + \left\{ (u_y^C + (x_j - x_c)u_T) - u_y^j \right\}^2 \right] \tag{3.9}$$

The mode values (u_x^C, u_y^C, u_T) were determined by minimizing the error J.

4.3.2 Three-dimensional mode

The eigenvalues obtained from the FDD technique by Iiyama and Kurita[11] are shown in Fig. 4.3. The horizontal and vertical axes represent the frequency and eigenvalue, respectively, and the figure shows eigenvalues from the first to fourth order. Focusing on the six peak frequencies for the first eigenvalue, i.e., 1.43, 1.51, 2.23, 3.97, 4.96, and 6.71 Hz, the corresponding eigenvectors are shown on the left side of Fig. 4.4 with respect to each location. Each eigenvector was normalized such that the maximum value was 1.0. The vertical axis represents the number of layers, and the horizontal axis represents the mode values in the components of the *TR* and *LG* directions. The right side of Fig. 4.4 shows the calculated three-dimensional eigenmodes. Here, the representative points of the three-dimensional eigenmodes are set to the centroid of the upper floor shown in Fig. 4.1(b). In this study, the calculated J was less than 1% of the following J_0 except for the third layer of the mode for 6.71 Hz. This indicates that the floor slabs can be considered to be sufficiently rigid during translational motion in the low-frequency range.

$$J_0(0,0,0) = \sum_{j=1}^{3} \left\{ (u_x^j)^2 + (u_y^j)^2 \right\} \tag{3.10}$$

From Fig. 4.4, the mode types for each peak frequency are determined and the characteristics of each mode are examined as follows.

The mode for 1.43 Hz is the first-order mode in the *TR* direction. The deformation is clearly larger on the east side than on the west side; the modal amplitude on the roof is 1.7 times larger at location NE than at location NW. Characteristically, the mode is clearly accompanied by torsional motion. The mode for 1.51 Hz is the first-order mode in the *LG* direction. The amplitudes at locations NW and NE are slightly different from each other in the component of the *TR* direction. This means that the mode was slightly coupled with torsional motion. The mode for 2.23 Hz is a typical first-order torsional mo-

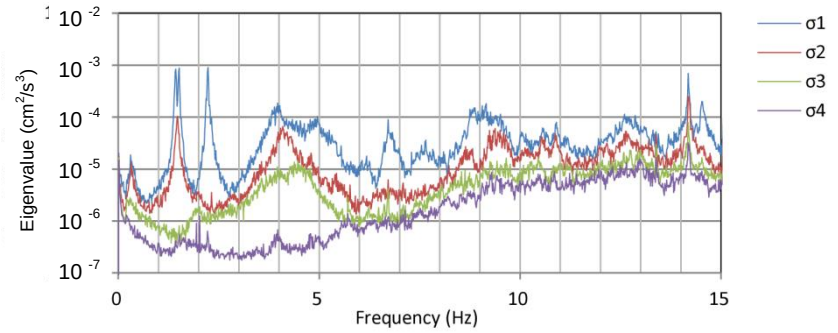

Figure 4.3. Eigenvalues of PSD matrix of response (eigenvalue spectrum)

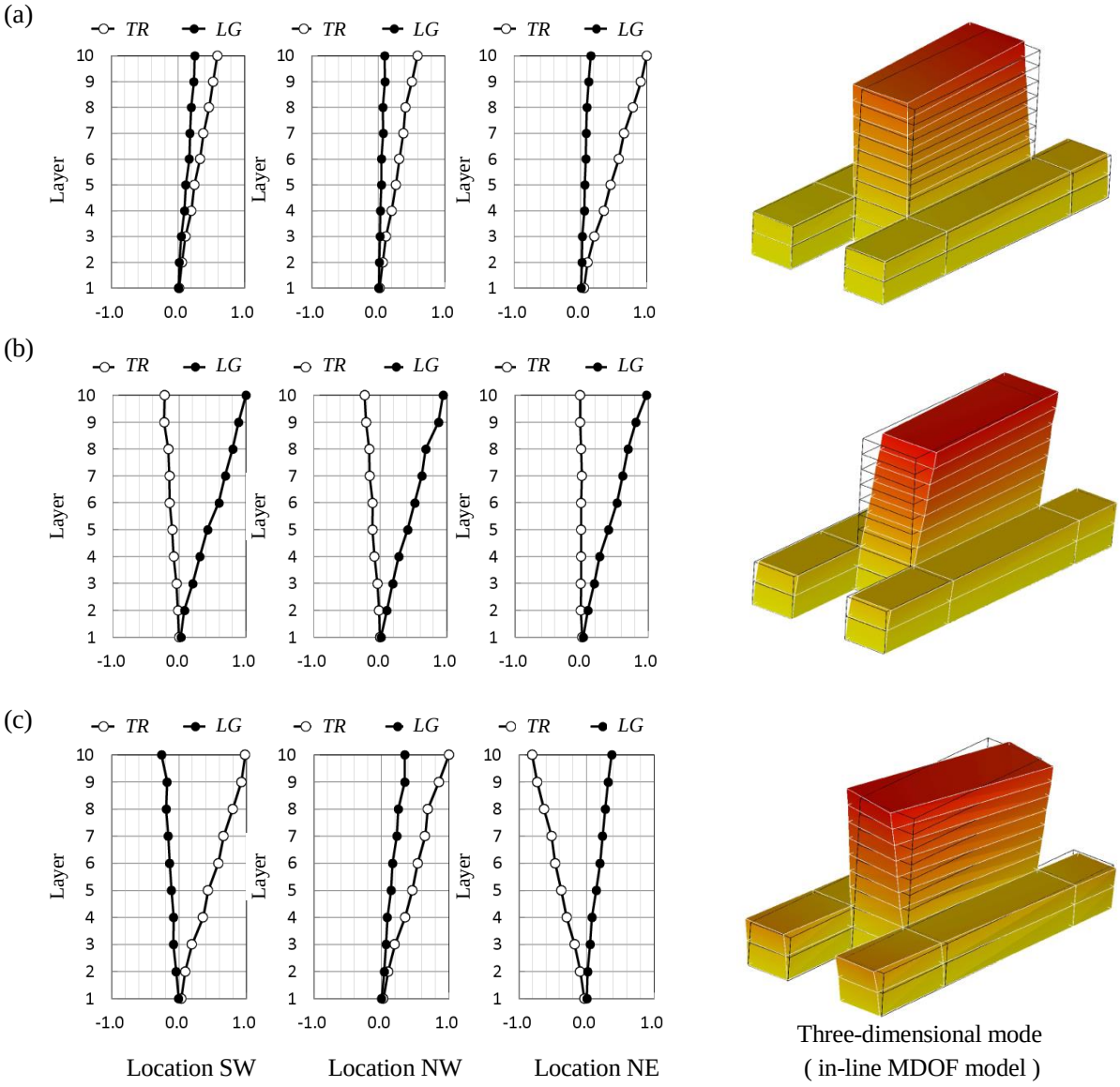

Figure 4.4(1) Identified modes at three locations (SW, NW, and NE) and in three-dimensional mode: (a) 1.43 Hz (first-order mode in *TR* direction, ⓑ1.51 Hz (first-order mode in *LG* direction), and (c) 2.23 Hz (first-order mode in rotational direction)

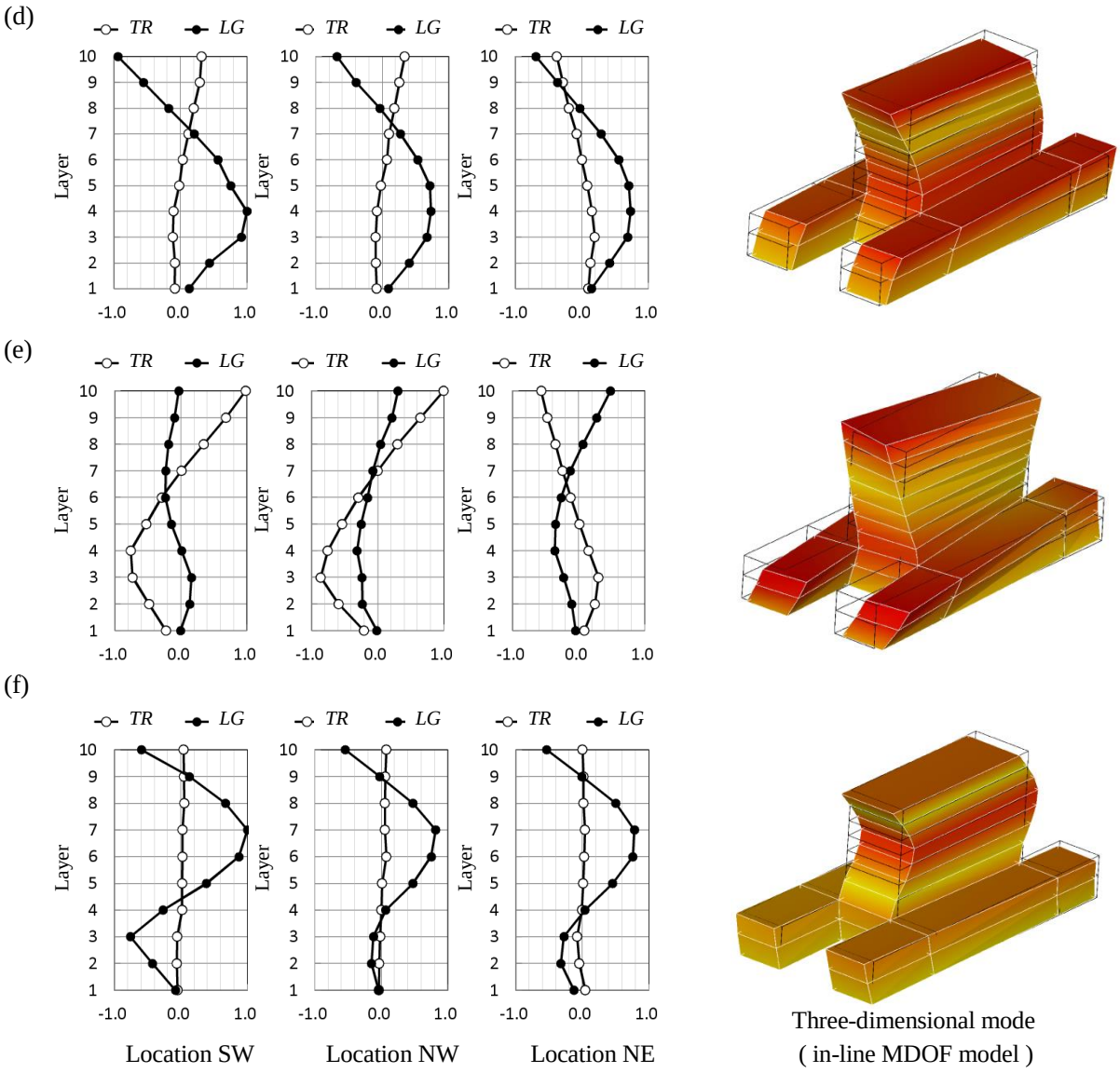

Figure 4.4(2) Identified modes at three locations (SW, NW, and NE) and in three-dimensional mode: (d) 3.97 Hz (second-order mode in *LG* direction), (e) 4.96 Hz (second-order mode in rotational direction), and (f) 6.71 Hz (third-order mode in *LG* direction)

de. From the mode shapes for each location, the deformation at location NE is found to be slightly smaller than that at location NW. This might be because of the slight translational motion in the *TR* direction.

The mode for 3.97 Hz is the second-order mode in the *LG* direction, which is coupled with the torsional motion. Focusing on the mode of component *LG*, the maximum value is different for each location. Thus, the mode shape seems to be complicated. Although the mode shape for 4.96 Hz is complicated, as shown in the modes for each location, it can be the second-order torsional mode based on the three-dimensional mode shape, the west side (SW and NW) of which moves in the opposite direction to the east side (NE). The amplitude of deformation in the *TR* direction is larger on the west side (SW and NW) than on the east side (NE). Although this tendency is different from that of the first-order mode, the cause of this difference is not yet clear.

The mode for 6.71 Hz is clearly the third-order mode in the *LG* direction. In contrast to the other modes, torsional deformation could not be found in the mode. On the other hand, the deformation of

component *LG* at location SW had a bent shape at the third layer, which was different from that at other locations. The cause of this difference and its relationship to damage are currently under investigation.

The second- and third-order modes in the *TR* direction could not be identified using this method, the reason for which is also under investigation.

4.4 Torsional characteristics of eigenmode and deformation ratio

Several translational modes seemed to be torsionally coupled. Therefore, the extent to which the torsional motion mixed with the translational mode was evaluated quantitatively by using the eigenmodes for the in-line MDOF model (the three-dimensional mode shown in Fig.4.4). In addition, the story deformation was detected for each eigenmodes from the modal deformation ratio between floors.

4.4.1 Torsional motion mixed in translational mode

The torsional component ratio ($RATIO_T$), which indicates the extent to which the torsional motion is mixed with the translational mode for the in-line MDOF model, was defined as follows:

$$RATIO_T = U_R / U_T$$

where U_R represents the torsional component at the edge of the layer in the *TR* direction, and U_T denotes the translational component at the representative point of the layer. The reference component of U_T was the component *TR* with respect to the transversal mode types and the component *LG* with respect to the longitudinal mode types. U_R was the angle of rotation multiplied by half of the length of the long side of the upper floor. Table 4.1 lists the $RATIO_T$ values calculated for the layer with the maximum mode value. $RATIO_T$ was clearly large for the first-order mode in the *TR* direction (25.5%) and for the second-order mode in the *LG* direction (17.8%). On the other hand, $RATIO_T$ was not very large for the first-order mode in the *LG* direction (10.0%). It was sufficiently small for the third-order mode in the *LG* direction.

In the case of the first-order mode in the *TR* direction, the difference between the mode values for the east and west side walls in the *TR* direction was 51%, which indicated that the mode was related to the development of torsional motion.

Table 4.1 Torsional component ratio ($RATIO_T$) for representative layer

Natural frequency	1.43 Hz	1.51 Hz	3.97 Hz	6.71Hz
Identified mode type	first-order (*TR*)	first-order (*LG*)	second-order (*LG*)	third-order (*LG*)
$RATIO_T$	25.5%	10.0%	17.8%	3.6%

4.4.2 Deformation ratio between floors

The deformation ratio of the i th-order eigenmode was defined as

$$ {}_i\delta_k^j = \left({}_i u_k^{j+1} - {}_i u_k^j \right) / h_j $$

where ${}_i\delta_k^j$ is the deformation ratio for the i th-order eigenmode with respect to the jth story for component k, h_j represents the story height between the jth and (j+1)th floors, and ${}_i u_k^j$ denotes the i th eigenmode with respect to the jth story for component k. Fig. 4.5 shows the identified mode shapes for the most dominant component in each mode (left) and its deformation ratio ${}_i\delta_k^j$ (right). With respect to the translational modes, not only the dominant component but also its perpendicular component are shown as a reference. Each mode was normalized such that the maximum value was equal to 1.0. The story height h_j was 6.15, 4.3, 3.8, 3.3, and 3.42 m for the first, second, third, fourth to eighth, and ninth stories, respectively.

The first-order mode groups (Fig. 4.5(a)–(c)) were characterized by the pattern of the deformation ratio ${}_i\delta_k^j$: they changed irregularly above the third floor in some ranges. Considering that (1) the

arrangement of structural members of the upper floors was uniform except for a part of the third floor and (2) the section sizes of each structural member gradually became smaller at higher floors, the distribution of ${}_i\delta_k^j$ is expected to uniformly change with the height above the third floor. Hence, the irregular patterns of ${}_i\delta_k^j$ are possibly related to the structural damage from earthquakes.

Note the analogy between the distribution patterns of ${}_1\delta_X^j$ (Fig. 4.5(a)) and ${}_1\delta_R^j$ (Fig. 4.5(c)). Both took larger values than the other floors at j = 3, 5, and 8. Meanwhile, ${}_1\delta_Y^j$ (Fig. 4.5(b)) took a larger value than the other floors at j = 5 and 8 and also had an irregular pattern. On the other hand, the patterns for the second- and third-order mode groups (Fig. 4.5(d), (e), and (f)) were more regular than those of the first-order modes.

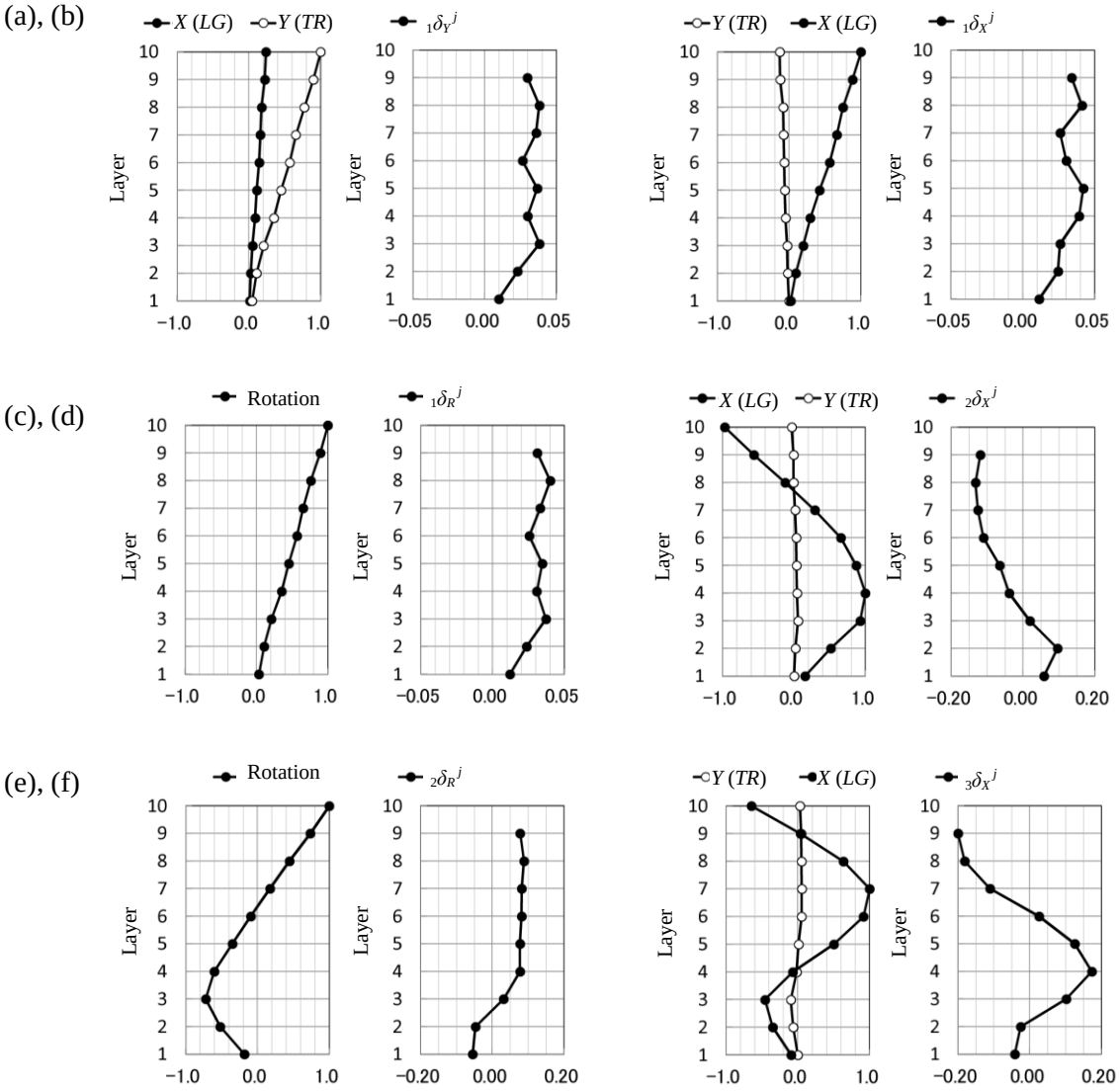

Figure 4.5. Mode shapes and modal deformation ratio at center of mass: (a) first-order mode (*TR*), (b) first-order mode (*LG*), (c) first-order mode (rotational), (d) second-order mode (*LG*), (e) second-order mode (rotational), and (f) third-order mode (*LG*)

4.5 Effect of difference in damping model on identified mode

Using the PSD matrix described in section 4.3, the eigenmodes were identified through two FDD methots by Brincker et al. (2001) , and by Iiyama and Kurita (2013); these methods are hereafter

referred to as the *conventional method* and *proposed method*, respectively. By comparing the identification results obtained from the two methods, the effect of the difference in the damping model on the identified mode were discussed.

The first singular values obtained through the conventional method and the first eigenvalues obtained through the proposed methods are shown in Fig. 4.6. It seemed that the singular values almost correspond to the eigenvalues. Fig. 4.7 shows the identified modes at location SW of component *LG*, with respect to the six peak frequencies mentioned in section 4.4.2. Each mode was normalized such that the maximum value was 1.0. The real part of the complex modes obtained using the conventional method seems to be in good agreement with the mode obtained using the proposed methods. If the eigenmode is regarded as the complex mode, the imaginary part of which is zero, we could say that the identified mode shapes were not influenced by the assumption of the damping models.

Next, the imaginary part of the complex mode obtained using the conventional method is analyzed. The imaginary parts are approximately zero for the first-order mode groups (Fig. 4.7(a)–(c)) and the second-order mode in the *LG* direction (Fig. 4.7(d)). On the other hand, small imaginary values appeared for two modes (Fig. 4.7(e) and (f)). It is believed that the imaginary part of the complex modes may appear in the high-frequency range.

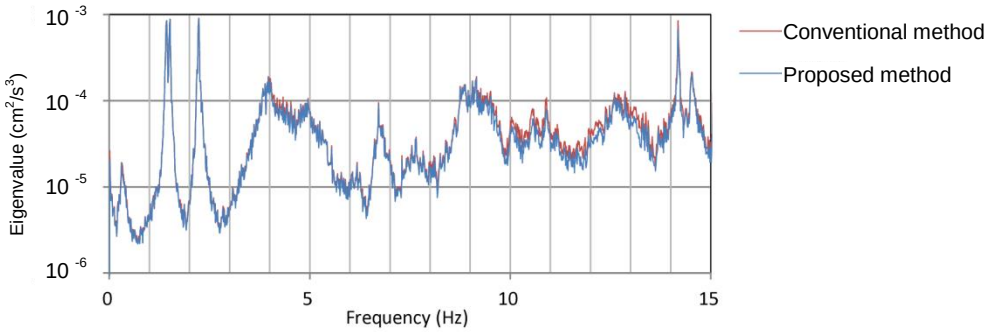

Figure 4.6. Comparison between first singular value (conventional method) and first eigenvalue (proposed method)

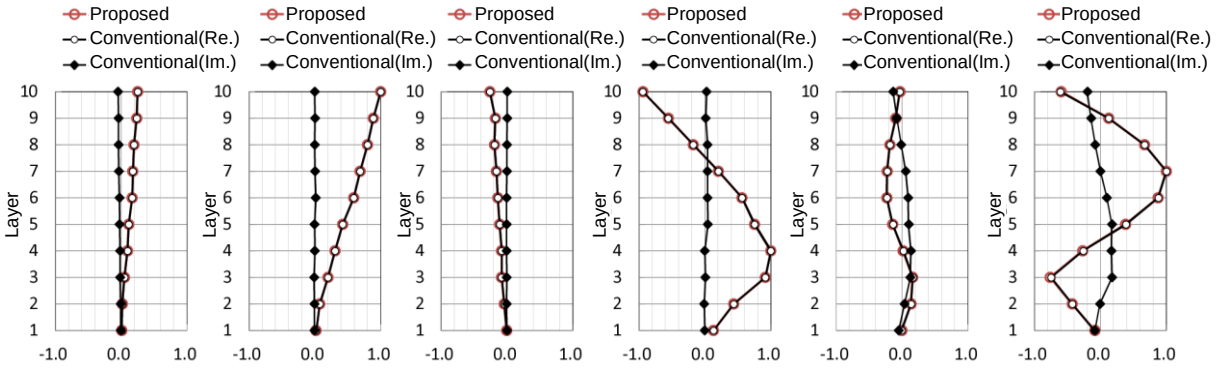

Figure 4.7. Comparison between identified modes obtained using conventional method and proposed method (location SW, component *LG*): (a) 1.43 Hz, (b) 1.51 Hz, (c) 2.23 Hz, (d) 3.97Hz, (e) 4.96Hz, and (f) 6.71 Hz

5. DISCUSSION

5.1 Amplitude dependence of frequency and change in frequency

In the building selected for this study, seismic observations[21)-24),26)], forced vibration tests[22),25)], and

ambient vibration measurements[25),27),28)] have been carried out after construction was completed. By analyzing the observation records, it was found that the stiffness of the building decreased considerably after the 1978 Miyagiken-oki earthquake and increased after the seismic retrofitting during 2000–2001. Motosaka et al.[27)] analyzed the amplitude dependence of the natural frequency in the period before the Miyagiken-oki earthquake in 1978 (Term-1), after the Miyagiken-oki earthquake in 1978 (Term-2), and after the seismic retrofitting (Term-3). The results are shown in Fig. 5.1. The vertical and horizontal axes of the figure represent the first natural period in the *TR* direction and the maximum deformation angle of the building, respectively. They clarified that the amplitude dependencies changed after significant stiffness reduction, indicating that the amplitude dependence differed for the three terms as shown in Fig. 5.1. In addition, they revealed that the natural periods obtained from ambient vibration records corresponded to the lower limit of the period range. Although the frequency would change at all times because of wind or other environmental factors, the amount of change can be ignored because it is sufficiently small in comparison to the change by earthquakes.

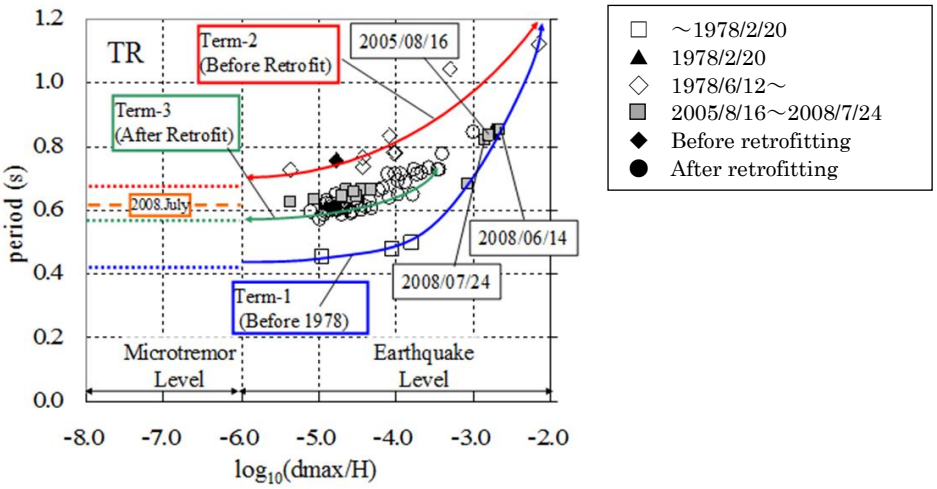

Figure 5.1. Amplitude dependence of natural frequency in *TR* direction [27)]

To evaluate changes in the natural frequency, only a series of frequencies obtained from ambient vibration records (hereafter called as f_{1amb}) were selected to remove the amplitude dependence of the natural frequency as much as possible. Table 5.1 lists the series of f_{1amb} values after the seismic retrofitting in 2000. The frequencies f_{1amb} were 1.48, 1.54, and 2.20 Hz in the *TR*, *LG*, and rotational directions, respectively, just before the seismic retrofitting. Because retrofitting increased the stiffness of the building, the frequencies in 2001 (after the retrofitting) increased to 1.74 Hz (17.6% increase), 1.85 Hz (20.1% increase), and 2.61 Hz (18.6% increase) in the *TR*, *LG*, and rotational directions, respectively. The mean rate of increase because of the retrofitting was 18.8%.

The changes in the frequency after the retrofitting were discussed in terms of the ratio (R_{freq}) of the frequency f_{1amb} to the frequency in 2001. The ratios just before the main shock of the Tohoku earthquake (period no.5) were 92.5% and 87.0% in the *TR* and *LG* directions, respectively. Thus, the frequencies had already decreased before the main shock. These decreases in f_{1amb} were apparently caused by the earthquakes that occurred during the period from 2001 (after the retrofitting) to 2011 (before the main shock). The differences between the ratios just before the main shock and after the main shock were 25.3% and 12.9% in the *TR* and *LG* directions, respectively. This result can explain the damage to the building after the Tohoku earthquake. Although the largest aftershock occurred on April 7, a change in frequency was not observed. On the other hand, the difference between the frequencies on May 3 and May 31 indicated that the stiffness of the building improved because of the emergency rehabilitation carried out in May. The increase in the frequency is approximately 50% of

the decrease in the frequency caused by the main shock. The value of(hereafter called as f_{1amb}) f_{1amb} on January 20, 2012 was slightly higher than that on May 31, 2012 after the emergency rehabilitation. This different could be caused by the removal of furniture and materials out of the building.

Although f_{1amb} was not measured for the torsional mode after 2001 for approximately 10 years, the changes in the frequency ratio for the torsional mode were clearly analogous to those for the translational mode. Therefore, the changes in f_1 for the torsional mode should have been the same as those for the translational modes. It is suggested that f_1 for the torsional mode traced the same changes as those for the transversal mode over the years.

Table 5.1. Changes in natural frequency based on ambient vibration measurements

Measurement period	First-order natural frequency f_{1amb}(Hz)		
	Translational mode		Torsional mode
	TR direction	*LG* direction	
No.1: In 2000, before retrofitting[25)]	1.48	1.54	2.20
No.2: Before No.3[25)]	1.72	1.75	2.60
No.3: In 2001, after retrofitting [25)]	1.74 [1.000]	1.85 [1.000]	2.61 [1.000]
No.4: March 9, 2011 [27)]	1.61 [0.925]	1.61 [0.870]	-
No.5: March 11, 2011 [27)]	1.61 [0.925]	1.61 [0.870]	-
2011 Tohoku earthquake			
No.6: March 19, 2011 [27)]	1.17 [0.672]	1.37 [0.741]	-
No.7: May 3, 2011 [27)]	1.17	1.37	-
(Emergency rehabilitation)			
No.8: May 31, 2011 [27)]	1.37 [0.787]	1.48 [0.800]	-
No.9: September 13, 2011	1.38 [0.793]	1.48 [0.800]	2.15 [0.824]
(Removal of furniture and materials out of the building)			
No.10: January 20, 2012	1.43 [0.822]	1.51 [0.816]	2.23 [0.854]

The numbers in [ ] are the ratio to the frequency after retrofitting in 2001

5.2 Relationship between modal properties and damage

The ratios of the torsional vibration included in the translational modes were different for modes of different orders. On the basis of this observation, the relationship between the modal properties and damage was studied.

As mentioned in section 2, the building showed torsional behavior only in the *LG* direction because of the unbalanced arrangement of the earthquake-resistant elements[22)]; however, it was verified that the unbalance in the *LG* direction had already been eliminated after the seismic retrofitting carried out in 2000[25)]. According to Fig. 4.4, the first translational mode in the *LG* direction was somewhat associated with torsional vibration. On the other hand, the first translational mode in the *TR* direction was clearly accompanied by torsional vibration. In addition, considering the difference in frequencies between the two directions before and after the main shock and the similarity in the slope distributions of the mode shape between the modes shown in Fig. 4.5(a) and (c), the stiffness reduction seemed to be caused by the main shock.

Because the amplitude for the east side is larger than that for the west side as shown in Fig.4.4(a), the damage on the east side might be more severe than that on the west side. In addition, the fact that the amount of recovery in the frequency by the emergency rehabilitation is approximately 50% of the amount of decrease in the frequency caused by the main shock implies that the stiffness of the side

wall was dominant in the total stiffness in the *TR* direction. Based on this fact, the largest stiffness reduction seemed to be have occurred in the east side wall.

5.3 Property of complex eigenmode identified from ambient vibration records

The influence of the damping model on the identified mode was evaluated by applying two FDD techniques: one for a non-proportional damping system[9], and the other for a proportional damping system[11]. It was confirmed that the real parts of the complex eigenmodes identified by the former FDD technique agreed with the eigenmodes identified by the latter FDD technique. In addition, the imaginary parts of the complex eigenmodes appeared only in the high-order modes.

According to a previous study by Kondo and Hamamoto[4], the variable coefficients for the imaginary part of the eigenmodes are statistically small whereas those for the real part are large. Their study indicates that the imaginary part possibly possesses lower reliability. Considering that the real part is principally dominant in the complex eigenmode even for the heavily damaged building and that the real parts of the complex eigenmodes agree with the eigenmodes identified by assuming a proportional damping system, the assumption of a proportional damping system for damage detection is valid. Further study is necessary to estimate the level of influence of the imaginary part of the complex eigenmodes on damage detection.

6. CONCLUSION

High-density-array measurement records of ambient vibration in a nine-story SRC building heavily damaged by the 2011 Tohoku earthquake were used to identify modal properties of the building through FDD techniques. On the basis of the study results, the following conclusions were drawn:

1) According to the change in the natural frequency of the first-order mode after the seismic retrofitting carried out in 2000, the natural frequency on January 20, 2011 was found to have been restored to approximately 60% of the amount of decrease in the frequency due to the main shock. Probably, 83% of the restoration was due to the emergency rehabilitation carried out only on the third floor and the rest due to the strengthening of concrete after emergency rehabilitation and the removal of furniture and materials out of the building. After the seismic retrofitting in 2001, the frequency reduced by 10% until the Tohoku earthquake. The reduction was probably caused by huge earthquakes that occurred during this period.
2) Several translational eigenmodes identified by FDD techniques were accompanied by torsional motion. Particularly, the maximum ratio of the torsional motion to the translational motion was 25.5% for the first-order eigenmode. This is most likely caused by the main shock and then the stiffness eccentricity in the transversal direction became large.
3) The deformation ratio of the i th-order eigenmode changed irregularly above the third floor in the first-order eigenmode, which is possibly caused by the main shock.
4) The real parts of the complex eigenmodes identified by the FDD technique assuming a non-proportional damping system agreed with the eigenmodes identified by the FDD technique assuming a proportional damping system.

   Considering that the real part is principally dominant in the complex eigenmode even for the heavily damaged building and that the real parts of the complex eigenmodes agree with the eigenmodes identified by assuming a proportional damping system, the assumption of a proportional damping system for damage detection is valid. The reason why the real parts of the complex eigenmodes coincide with the eigenmodes identified by assuming a proportional damping system and the reason for the appearance of the imaginary part of the complex eigenmodes in high-order modes are under investigation.

ACKNOWLEDGEMENT

The authors are grateful to NEWJEC Inc. (Technology Developing Group), NTT Facilities (Research & Development Headquarters), Yamanaka Laboratory of the Tokyo Institute of Technology, Nagano Laboratory of the Tokyo University of Science, and Toshinawa Laboratory of Meisei University for lending us portable accelerometers. We would also like to thank the technical staff of Tohoku University—Tatsuo Sasaki, Associate Prof. Susumu Ohno, and Prof. Takeshi Sato—for their valuable support during the measurements.

REFERENCES

1) Tamura Y, Yoshida A et al.: Ambient vibration testing and modal identification of a 15-story office building due to FDD technique: Part 1 Ambient vibration testing and modal identification due to FDD, Summaries of Technical Papers of Annual Meeting of Architectural Institute of Japan, 2000, pp.979-980. (in Japanese)
2) Hamamoto T and Inoue R: Member damage detection of multistory buildings using parallel model identification, Journal of Structural and Construction Engineering, Vol.655, 2010, pp.1661-1670. (in Japanese)
3) Saito T: Probabilistic damage estimation through structural identification, Journal of Structural and Construction Engineering, Vol.557, 2002, pp.93-100. (in Japanese)
4) Kondo I and Hamamoto T: Damage detection of multi-storey buildings using random response data from shaking table tests, Journal of Structural and Construction Engineering, Vol.473, 1995, pp.67-74. (in Japanese)
5) Hamamoto T and Kondo I: Two-stage damage detection of eccentric multistory buildings using vertical and horizontal searching, Journal of Structural and Construction Engineering, Vol.519, 1999, pp.21-28. (in Japanese)
6) Hamamoto T, Oeki Y and Miyoshi T: Damage detection of multistory buildings using active identification scheme, Journal of Structural and Construction Engineering, Vol.539, 2001, pp.51-56. (in Japanese)
7) Hamamoto T, Morita T and Teshigawara M: Story damage detection of multistory buildings using natural frequency shifts of multiple modes, Journal of Structural and Construction Engineering, Vol.560, 2002, pp.93-100. (in Japanese)
8) Kanazawa K and Matsui T: ARMAMA model for spectral analysis and modal identification, Journal of Structural and Construction Engineering, Vol.554, 2002, pp.71-78. (in Japanese)
9) Brincker R, Zhang L and Andersen P: Modal identification of output-only systems using frequency domain decomposition, Smart Material and Structures, Vol.10, 2001, pp.441-445.
10) Zhang L-M, Wang T and Tamura Y: A frequency-spatial domain decomposition (FSDD) technique operational modal analysis, Mechanical Systems and Signal Processing, Vol.24, Issue 5, 2009, pp.1227-1239.
11) Iiyama K and Kurita S: Development of the theory of modal identification for proportional viscous damping system by frequency domain decomposition, Proceeding of Architectural Research Meetings**,** Kinki, Vol.52, 2012, pp.109-112. (in Japanese)
12) Izumi M, Katsukura H and Tobita J: Properties of ambient vibration system of structures, Journal of Structural and Construction Engineering, Vol.409, 1990, pp.83-92. (in Japanese)
13) Ishibashi T and Naito Y: Influence of wind force on system identification of tall buildings during microtremors, Journal of Structural and Construction Engineering, Vol.464, 1994, pp.71-80. (in Japanese)
14) Naito Y and Ishibashi T: Transfer function deformation mechanism due to wind force effect on buildings during microtremors, Journal of Structural and Construction Engineering, Vol.497, 1997,

pp.57-64. (in Japanese)
15) Fukuwa N, Yamasaki Y, Kojima Y and Tobita J: Differences of dynamic responses of buildings due to ambient vibration, strong wind and seismic ground motion based on observed data, Journal of Structural and Construction Engineering, Vol.598, 2005, pp.61-68. (in Japanese)
16) Nakamura M and Yasui Y: Damage evaluation of a steel structure subjected to strong earthquake motion based on ambient vibration measurements, Journal of Structural and Construction Engineering, Vol.517, 1999, pp.61-68. (in Japanese)
17) Shiga T, Shibata A, Shibuya J and Takahashi J: Observations of strong earthquake motions and nonlinear response analyses of the building of Architectural and Civil Engineering Department, Tohoku University, Transactions of the Architectural Institute of Japan, Vol.301, 1981, pp.119-129. (in Japanese)
18) Yamaguchi I: Seismic retrofit of the building of architectural and civil engineering department、Aoba kougyou-kai kaihou Vol. 45, 2001 (in Japanese)
19) Sakota T, Matsukawa K, Miura K et al.: Damages and restoration of school of engineering of tohoku university (Aobayama campus) strucked by the 2011 off pacific coast tohoku earthquake, JAEE annual conference, 2011, pp.46-47. (in Japanese)
20) Cho K. : -Shingo Shori No Tame No Senkei Daisu- (Linear algebra for signal processing), Morikita Publishing Co., Ltd., 2008 (in Japanese)
21) Shiga T, Shibata A and Ueno K: Earthquake response observation of the Building of architectural and civil engineering department of tohoku university、Research report of architectural department of tohoku University, Vol.14, 1972 (in Japanese)
22) Shiga T, Shibata A and Shibuya J: Dynamic properties and earthquake response of a 9 story reinforced concrete building, Proc. 5th WCEE, Roma, 1973, pp.2680-2683. (in Japanese)
23) Ali N and Motosaka M: Dynamic response characteristics of the actual building subjected to the incident waves generated from air gun impactor, AIJ Journal of Technology and Design, Vol.12, 2001, pp.47-52.
24) Motosaka M, Mitsuji K et al.: Change of dynamic characteristics of a damaged building before, during, and after the 2011 Off Pacific Coast Tohoku Earthquake, Summaries of Technical Papers of Annual Meeting of Architectural Institute of Japan, 2011, pp.45-46. (in Japanese)
25) Motosaka M, Suzuki H and Sato T: Evaluation of seismic damage and reinforcement effects of an existing building based on forced vibration tests before and after the reinforcement work, The Earthquake Engineering Symposium Proceedings, Japan, Vol.11, 2002, pp.2015-2020. (in Japanese)
26) Tsamba T and Motosaka M: Investigation of dynamic behavior of a damaged 9-story building during the 2011 off the Pacific Coast Tohoku Earthquake, JAEE annual conference, 2011, pp.44-45. (in Japanese)
27) Motosaka M, Mitsuji K and Tsamba T: Long-term monitoring of amplitude dependent dynamic characteristics of a damaged building during the 2011 Tohoku Earthquake, Summaries of technical papers of 30th annual meeting, Japan society for natural disaster science, 2011, pp.161-162. (in Japanese)
28) Motosaka M: Study on Damage and strengthening effects of building structures based on vibration tests using impactor machines、Grant-in-Aid for Scientific Research (C) , Progress report, 2003.5. (in Japanese)

(Original Japanese Paper Published: November, 2012)
(English Version Submitted: December 24, 2014)
(English Version Accepted: February 9, 2015)